Photosynthesis Within Large-Scale Ecosystem Models

CHAPTER · DECEMBER 2008

DOI: 10.1007/978-1-4020-9237-4_19

2 AUTHORS:

Stephan A Pietsch
International Institute for Applied Systems…
41 PUBLICATIONS **351** CITATIONS
SEE PROFILE

Hubert Hasenauer
University of Natural Resources and Life Sci…
121 PUBLICATIONS **1,445** CITATIONS
SEE PROFILE

Chapter 19

Photosynthesis Within Large-Scale Ecosystem Models

Stephan A. Pietsch and Hubert Hasenauer*
Institute of Silviculture
Department of Forest and Soil Sciences, University of Natural Resources and Applied Life Sciences, Peter-Jordan-st. 82, A-1190 Vienna, Austria

Summary

In large scale ecosystem models photosynthesis interacts with other ecosystem processes such as transpiration, evaporation, soil hydrology, assimilate allocation, growth and maintenance respiration, biomass mortality, heterotrophic respiration, decomposition, mineralization, and nutrient leaching and

* Author for correspondence, e-mail: hubert.hasenauer@boku.ac.at

A. Laisk, L. Nedbal and Govindjee (eds.), Photosynthesis in silico: Understanding Complexity from Molecules to Ecosystems, pp. 441–464.

volatilization. These processes are of biological, physicochemical and hydro-geological nature and are summarized under the term biogeochemistry. This chapter explains the relations among photosynthesis and the biogeochemical cycles of carbon, nitrogen, water and energy and describes how these complex cycles are integrated in a modeling environment by outlining: (i) the model algorithm, (ii) the mechanistic detail of the implementation of processes such as photosynthesis, groundwater infiltration and biomass mortality, (iii) the role of model parameters, (iv) the properties of model drivers and (v) the constraints provided by the temporal resolution of the model implementation. Emphasis is laid on the single steps of model application, from model initialization and the consideration of historical land use and land use change to the simulation of a current ecosystem. Tests of model sensitivity and the necessity of model validation versus field observations are explained. Besides statistic validation procedures, which provide accuracy and precision of model predictions, methods from higher mathematics are introduced to analyze model dynamics. These methods allow the distinction between stable and unstable model behavior. In scenario simulations such as climate change impact studies no observations are available to assess the accuracy and precision of model predictions and model stability becomes the key criterion to judge the predictive value of model outputs. If model dynamics remain stable then model predictions remain valid, if, however, model dynamics become unstable then the interpretation of model results is meaningless. Next, examples of model application are provided dealing with (i) virgin forest conditions unaffected by direct human impact, (ii) model calibration and validation for production forests, where human impact affected species composition and site quality and (iii) the assessment of model dynamics and how the results of such analyses may be interpreted. Concluding remarks emphasize the central position of photosynthesis, the importance of field observations for model validation and the key role of assessing model dynamics in scenario studies.

I. Introduction

Large scale ecosystem models describe the fluxes of carbon, nitrogen, water and energy within ecosystems. Photosynthesis and related processes are central as they transform inorganic carbon into carbohydrates, thus providing the organic backbone for structural and functional molecules of living organisms. In large scale ecosystem models other processes such as allocation of assimilates for growth of shoots and roots, growth and maintenance respiration, phenological biomass turnover, mortality, decomposition, mineralization, denitrification, evapotranspiration, soil water outflow and flooding, surface reflectance or heat transfer must be considered in order to capture the growth and decay following mortality within these ecosystems. These processes are of biological, physicochemical, and hydro-geological nature and may be summarized by the term biogeochemistry. All of these processes directly or indirectly depend on photosynthesis (Fig. 19.1).

Within ecosystem models, all processes must be addressed at a similar level of detail in order to ensure a balanced representation of reality (Waring and Running, 1998). Differences in the level of detail and/or temporal and spatial resolution may lead to biased and inconsistent predictions, given that a single modeled process may dominate the system in such instances. For example, a well balanced approach has to prevail between the treatments of photosynthesis and transpiration so that the trade-off between the carbon gain and water loss, influenced by stomatal conductance, is properly addressed. Stomatal conductance and transpiration are affected by

Abbreviations: GPP – gross primary production: net plant C uptake from photosynthesis (kg C m^{-2}); LAI – leaf area index: leaf area per m^2 ground area (m^2 m^{-2}); NEE – net ecosystem exchange: rate of C sequestration within an ecosystem (kg C m^{-2}); NPP – net primary production: GPP minus plant respiration (kg C m^{-2}); PHAR – photosynthetically active radiation: part of the solar radiation that is utilized for photosynthesis (W m^{-2}); R_h – heterotrophic respiration: C release during decomposition processes (kg C m^{-2}); Rubisco – Ribulose 1,5-bisphosphate carboxylase/oxygenase; PEP – phosphoenol pyruvate; VPD – vapor pressure deficit: difference between the partial pressure of atmospheric water vapor at 100% relative humidity and the partial pressure of atmospheric water vapor at actual relative humidity (Pa)

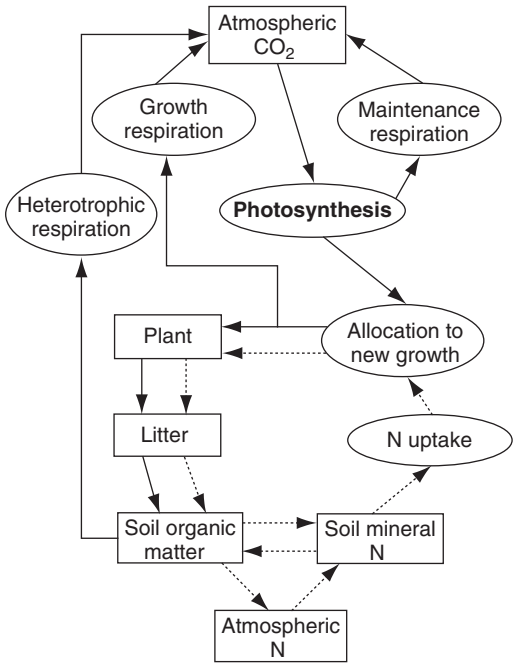

Fig. 19.1. Simplified schematic of the fluxes (arrows), state variables (boxes) and processes (ellipses) considered in large scale ecosystem models. Solid lines indicate carbon fluxes, dotted lines indicate nitrogen fluxes, water and energy pools and fluxes were left out for clarity (Thornton et al., 2002, modified)

issues of soil hydrology. The trade-off between soil moisture and litter decomposition affects mineral nitrogen release. Soil mineral nitrogen content constrains plant growth and affects the leaf area available for radiation absorption. Radiation absorption provides the energetic source and determines the carbon assimilation potential of photosynthesis.

In the previous chapters of this book, photosynthesis is modeled with a high level of detail. Conceptually, this would require that the other processes, such as transpiration, groundwater infiltration, biomass turnover or decomposition, must be treated in a comparable detail. This increases computation time, and as such, data handling ability may become the limiting factor in large scale model applications. Another difficulty may be the comparison of model output to field observations, since field observations are usually not available at the same level of detail as modeled processes.

The purpose of this chapter is to demonstrate how complex large scale ecosystem models may be applied and tested versus field observations. This chapter will (i) give a description of the biogeochemical cycles in order to address the mass and energy balance, (ii) describe the structural features of the models and (iii) explain the steps of model application.

II. Biogeochemical Cycles

Biogeochemical cycles (BGC) describe the transformation of energy and matter within ecosystems (Waring and Running, 1998). Using solar short wave radiation (photosynthetically active) and inorganic matter, autotrophic processes produce organic matter charged with internal chemical energy. At the end of the cycle, heterotrophic decay releases long wave radiation (heat) and inorganic matter. Carbon, nitrogen, water and energy are considered as the key components within the modeling environment.

A. Carbon Cycle

The carbon source for photosynthesis is provided by CO_2, whose concentration within the leaves depends on the atmospheric concentration and stomatal conductance. The rate of photosynthesis depends on the amount of the primary carbon fixing enzyme (ribulose 1,5-bisphosphate carboxylase/oxygenase, Rubisco, in C_3 plants and phosphoenol pyruvate, PEP, carboxylase in C_4 and CAM plants). The reaction rate is calculated using enzyme kinetics, leaf temperature, absorbed radiation and photosynthetic electron transport rate according to different models (e.g. for C_3, de Pury and Farquhar, 1997; for C_4, Laisk and Edwards, 2000). Leaf Area Index (LAI, m^2 leaf area per m^2 ground area) is calculated from carbon allocated to leaves multiplied by the specific leaf area (m^2 leaf area per kg leaf carbon). LAI controls canopy radiation absorption, which provides the energetic source for photosynthetic carbon fixation.

Gross Primary Production (GPP) is the rate of photosynthesis minus the leaf maintenance respiration during daytime (R_{md}) which is calculated as a function of leaf nitrogen concentration (Ryan, 1991) and daytime length. Net Primary Production (NPP) is based on GPP minus autotrophic respiration (R_a). The latter

includes the maintenance respiration of (i) leaves during nighttime, (ii) all other tissues during the whole day and (iii) growth respiration (R_g), which is a function of the amount of carbon allocated to different plant structural compartments (Penning de Vries, 1974). NPP is partitioned into the leaves, roots and stems as a function of dynamic allocation patterns, considering possible limitations in the availability of, and the competition for, nitrogen.

Net Ecosystem Carbon Exchange (NEE) provides the balance between NPP and heterotrophic respiration (R_h). R_h depends on the decomposition activity, which is regulated by soil temperature and soil moisture, as well as the amount of decomposition material. The ecosystem acts as a carbon sink when the amount of carbon released via R_h is lower than NPP. The ecosystem acts as a net carbon source when R_h exceeds NPP due to high amounts of decomposable material and/or high decomposition activity. The amount of decomposable material is governed by the mortality rate of vegetation biomass. Mortality thereby links living biomass with litter and soil organic matter and influences the total ecosystem carbon content.

B. Nitrogen Cycle

Nitrogen (N) sources include deposition, nitrogen fixation and decomposition fluxes. Plant uptake, microbial immobilization and volatile and leaching losses are nitrogen sinks. Plant N demand is determined by NPP. The immobilization demand is calculated from the decomposition rate and depends on the amount of decomposable material. Decomposition rates of litter and soil carbon pools change with soil temperature (Lloyd and Taylor, 1994) and soil moisture (Andren and Paustian, 1987). These factors determine the magnitude of N mineralization from decomposition and influence the heterotrophic respiration.

A small portion of N is released into the atmosphere during mineralization by denitrification. Nitrogen may percolate down to groundwater or it may be released into the atmosphere via denitrification, when soil mineral nitrogen content exceeds the sum of microbial and plant nitrogen demand. If the sum of microbial and plant nitrogen demand is equal to the amount of available soil mineral nitrogen, no denitrification occurs (Aber, 1992).

Plants and microorganisms compete for soil mineral nitrogen when the amount of available soil mineral nitrogen is lower than the demand. While plant demand depends on NPP, microbial demand depends on (i) the amount of material available for decomposition and (ii) the decomposition rate, which depends on the temperature and soil moisture (Andren and Paustian, 1987; Lloyd and Taylor, 1994). The availability of mineral N and the sum of plant and microbial N demand defines a supply/demand ratio, which is used for the allocation of N available for uptake by plants and microorganisms.

C. Water Cycle

Water enters terrestrial ecosystems from (i) the atmosphere by rainfall, (ii) the snowpack by melting, (iii) lateral inflows like flooding, and (iv) the ground water table by soil water recharge. Rainfall is partially intercepted by the canopy. If the amount of rainfall exceeds the potential canopy interception, it is routed to the soil water pool. Water is released from a snow pack and adds to the soil water pool, if the energy input from temperature and radiation exceeds the energy of melting. Lateral water inflow occurs when water input from rainfall or snowmelt exceeds the capacity of standard water discharge routes, e.g. brooks and rivers.

The upper limit for soil water content is the soil porosity, which equals the total volume of soil pores. Ground water recharge, of the soil volume accessible by plants, occurs only if the soil water content falls below the field capacity. Field capacity is equal to the soil water content when the gravitational force is equal to the retention force of soil water potential and is lower than soil water saturation. Below the field capacity, the upward pressure of the soil water potential exceeds the downward pressure from gravitation. The amount of ground water ascent is defined by the net upward force and the soil hydraulic conductivity, which depend on soil texture and soil water content (Pietsch et al., 2003).

Water leaves the ecosystem by plant transpiration, soil evaporation, snow sublimation and soil water outflow. Plant transpiration depends on the atmospheric vapor pressure deficit, leaf

temperature and water potential, and stomatal conductance to water vapor. Stomatal conductance is regulated by the leaf water potential, atmospheric vapor pressure deficit and temperature. Additionally, canopy transpiration depends on the wind speed. Evaporation of soil water is governed by the atmospheric vapor pressure deficit and the temperature. Sublimation of snow water is determined by the radiation energy input. Soil water outflow includes all water, which is above soil water saturation and a proportion of soil water above field capacity (Chang, 2003).

D. Energy Cycle

Energy enters ecosystems as solar radiation and sensible heat of atmospheric temperature. A portion of solar radiation is reflected by plant surfaces, whereas another part is absorbed by leaves and other plant organs. The remaining radiation is transmitted to the snow pack or bare soil, where another proportion is reflected and the rest is absorbed. The sum of reflected radiation is due to the ecosystem type, vegetation cover, snow cover and the soil type; it is called the albedo. In addition to the energy loss via the albedo effect, energy also leaves the ecosystem as latent heat during processes such as snow sublimation, transpiration and evaporation of water intercepted by the canopy or water stored in the soil. Radiation absorption by leaves and the temperature of the surrounding air, determine the leaf temperature. This affects the enzyme activity of carbon assimilation. The mean air temperature over longer durations of time (days, weeks) determines soil temperature, which, in turn, affects the activity of decomposition enzymes. Air temperature also affects stomatal conductance and regulates the water vapor flux density and the energy loss due to latent heat transfer between vegetation and the atmosphere.

E. Interactions Between Cycles

As is evident from the description of the carbon, nitrogen, water and energy cycles, none of them can be calculated as a single, linear, causal relationship. Among these cycles, multiple interactions exist and have to be considered within modeling in order to mimic nature as closely as possible. Conceptually, these interactions are organized as feedback loops, making the modeled ecosystem behave in a strongly nonlinear fashion.

An important trade-off exists between photosynthetic carbon gain and transpiration water loss. Carbon availability for photosynthesis depends on the partial pressure of atmospheric CO_2 and the stomatal conductance. The partial pressure of atmospheric CO_2 is a physical function of elevation. Stomatal conductance is driven by an atmospheric vapor pressure deficit and the leaf water potential. Leaf water potential depends upon soil water potential, and it is derived from the texture of the soil and the soil water content. Soil water content is influenced by water input via precipitation and results from the amount of rainfall, which is not intercepted by the canopy. Canopy size depends on the amount of carbon allocated to leaves and it is regulated by the amount of carbon which is assimilated via photosynthesis (Pietsch and Hasenauer, 2005b).

Next, there is the trade-off between photosynthetic carbon gain and nitrogen availability. Carbon assimilated by photosynthesis is incorporated into structural and functional biomolecules which exhibit a certain N/C-ratio. Wood has a low N/C-ratio and thus has a low demand of nitrogen per unit carbon. Leaves have a high N/C-ratio due to their high content of enzymatic proteins. The carbon fixing protein Rubisco may account for up to 30% of nitrogen in the leaves alone (Evans, 1989). Nitrogen availability constrains photosynthetic carbon fixation.

Another example is biomass turnover and mortality, which follow seasonal and plant life-time cycles. Both influence the litter availability for decomposition at a certain time of the season or at a certain time during the plant life cycle. The more biomass is available for decomposition, the higher is the microbial nitrogen demand, which lowers the amount of nitrogen for plant uptake. Decomposition enhances ecosystem nitrogen loss due to denitrification-induced volatile nitrogen release. Low availability of nitrogen for plant uptake particularly affects leaf growth due to the high N/C ratio of leaves and their resulting high demand for nitrogen per carbon assimilated via photosynthesis. A decreased growth rate of leaves means less radiation is intercepted by the leaves and a resulting lower rate of photosynthetic carbon assimilation is observed. Less carbon assimilation leads to a lower plant nitrogen demand.

Nitrogen released from enhanced decomposition will gradually increase soil mineral nitrogen content and cause volatile and leaching losses of mineral nitrogen. With time the amount of decomposable biomass will decrease and microbial nitrogen demand will decline. More nitrogen will be available for plant uptake at the start of the next season or new plant life cycle and plant growth is favored. Biomass is built up until turnover or mortality occurs, and the amount of decomposable material increases again (Pietsch and Hasenauer, 2006).

Decomposition activity depends on soil moisture and temperature. When plant growth is limited by low nitrogen availability, canopy size is reduced and less radiation and precipitation is intercepted by plant surfaces. This increases the soil temperature and moisture, which both enhance decomposition. This may increase N-leaching as well as soil evaporation depending on the precipitation regime. Soil evaporation decreases soil moisture, which, in turn, regulates decomposition activity (Merganicova et al., 2005).

These four examples illustrate the multiple feedback processes among the cycles of water and carbon, carbon and nitrogen, nitrogen demand of decomposers and plants and their link to the energy cycle. All together the biogeochemical cycles resemble a complex network of feedback loops. None of the cycles can be modeled without considering the others.

III. Models of Biogeochemical Cycles

Within large-scale BGC modeling, an ecosystem is viewed as a set of ecosystem compartments (the atmosphere, leaves, stems, roots, litter, soil) carrying water, carbon and nitrogen pools as well as energy. The sizes of the pools define the state of an ecosystem. Changes in state depend on the fluxes of energy and matter amongst the pools. These fluxes govern the energy and matter balance within a given ecosystem. Pools as well as fluxes are restricted by the interactions among the cycles of energy and matter (Section II.E). This section describes (i) the general model algorithm, (ii) the technical implementation of a few processes governing the fluxes of energy and matter, (iii) the model parameters defining the interactions among the pools and fluxes, (iv) the dynamic and static input variables driving/constraining flux dynamics among the pools and (v) the constraints provided by the temporal resolution of models.

A. Model Algorithm

Similar to nature, the present state of an ecosystem is determined by its state in the past and the forces driving the changes from the past to the present state. In large scale ecosystem models this classical recursion is addressed as follows: after each simulated time step the sizes of the different pools are changed by the fluxes. Hence, the size of a pool depends on its present state and the balance between influx and efflux. The general production formula may be expressed as follows:

$$\Theta_{T_{n+1}} = f(\Theta_{T_n}, \varphi_{T_n}, \alpha, \sigma), \tag{19.1}$$

where $\Theta_{T_{n+1}}$ is the set of pool sizes at time T_{n+1}, Θ_{T_n} is the set of pool sizes one recursion step earlier, φ_{T_n} is the set of model drivers at time T_n (which induce the fluxes among the pools and thereby cause the changes from Θ_{T_n} to $\Theta_{T_{n+1}}$), α is the model parameter set encapsulating specific properties of the modeled ecosystem, σ is the set of physical site properties, and f is the functional algorithm of the model implementation.

The modeled state of an ecosystem at a time T_{n+1} depends on its state at time T_n, and so forth:

$$\Theta_{T_0} \rightarrow \Theta_{T_1} \rightarrow \ldots\ldots\ldots \rightarrow \Theta_{T_{n-1}} \rightarrow \Theta_{T_n} \rightarrow \Theta_{T_{n+1}}. \tag{19.2}$$

Accordingly any Θ_{T_n} relies on the values of state at time T_0, i.e. the initial conditions. In some situations the initial conditions may be available from previous measurements, e.g. sites of long-term research. In general the information about the initial conditions is either missing or incomplete. While e.g. the age of forest stand may be known (or determined on site from increment cores) the state of the plot before stand establishment is often unknown. It may have been a virgin forest, a coppice forest used for fuel wood which in turn may have been degraded due to extensive litter raking, or it may also have previously been an abandoned meadow, pasture or a piece of arable land.

B. Modeled Processes

1. Photosynthesis

The equations for calculating photosynthetic carbon assimilation are based on the work of Kuehn and McFadden (1969), Woodrow and Berry (1980), Farquhar et al. (1980), Wullschleger (1993) and de Pury and Farquhar (1997). Net photosynthetic carbon assimilation at the leaf level is given by the equation:

$$A = \min(A_v, A_j) - R_{ml}, \tag{19.3}$$

where A_v is the Rubisco limited rate of photosynthesis, A_j is the electron transport limited rate of photosynthesis and R_{ml} is the leaf maintenance respiration. A_v is calculated using

$$A_v = \frac{V_{max} \cdot (P_C - \Gamma)}{P_C + K_C \cdot (1 + \frac{P_O}{K_O})}, \tag{19.4}$$

where V_{max} is the Rubisco maximum rate per unit leaf area, P_C is the partial pressure of CO_2 within the leaf, Γ is the CO_2 compensation point of photosynthesis, K_C is the Michaelis-Menten constant of Rubisco for CO_2, P_O is the partial pressure of O_2 and K_O is the Michaelis-Menten constant of Rubisco for O_2. V_{max} is defined as:

$$V_{max} = \frac{N_l \cdot N_{lR} \cdot Act_R}{N_R}, \tag{19.5}$$

whereby N_l is the leaf N content per unit leaf area, N_{lR} is the proportion of leaf N contained in Rubisco, N_R is the fraction of N in Rubisco and Act_R is the Rubisco activity. Act_R is calculated from the Rubisco activity at 25°C (Act_{R25}), the Q_{10} for Rubisco activity (Q_{10R}) and temperature (t):

$$Act_R = Act_{R25} \cdot Q_{10R}{}^{\frac{t-25}{10}} \text{ if } t > 15°C, \tag{19.6}$$

$$Act_R = Act_{R25} \cdot Q_{10R}{}^{\frac{t-15}{10}} \text{ if } t \leq 15°C. \tag{19.7}$$

The Michaelis-Menten constants K_O and K_C also exhibit temperature dependence and are calculated from their respective values at 25°C (K_{O25}, K_{C25}) and the respective Q_{10}-values

$$K_O = K_{O25} \cdot Q_{10O}{}^{\frac{t-25}{10}}, \tag{19.8}$$

$$K_C = K_{C25} \cdot Q_{10C}{}^{\frac{t-25}{10}} \text{ if } t > 15°C, \tag{19.9}$$

$$K_C = K_{C25} \cdot Q_{10C}{}^{\frac{t-15}{10}} \text{ if } t \leq 15°C. \tag{19.10}$$

The CO_2 compensation point (Γ) is calculated under the assumption that the ratio of maximal oxgenase and carboxylase activity of Rubisco equals 0.21 (Wullschleger, 1993):

$$\Gamma = \frac{0.21 \cdot P_O \cdot K_C}{2 \cdot K_O}. \tag{19.11}$$

The electron transport-limited rate of photosynthesis A_j is calculated as

$$A_j = \frac{J \cdot (P_C - \Gamma)}{4.5 \cdot P_C + 10.5 \cdot \Gamma}. \tag{19.12}$$

Here J is the rate of electron transport per unit leaf area and is given by

$$J = J_{max} + \text{PHAR} \cdot \frac{p_{abs}}{ppe} - \sqrt{\frac{(-J_{max} - \text{PHAR} \cdot \frac{p_{abs}}{ppe})^2 - 4 \cdot 0.7 \cdot J_{max} \cdot \frac{p_{abs}}{ppe}}{2 \cdot 0.7}}, \tag{19.13}$$

where J_{max} is the potential rate of electron transport defined as

$$J_{max} = 2.1 \cdot V_{max}. \tag{19.14}$$

PHAR is photosynthetically active radiation, p_{abs} is the leaf absorption coefficient defining the fraction of PHAR effectively absorbed by the leaves and *ppe* is the amount of photons absorbed by photosystem II per electron transported.

2. Ground Water Infiltration

Infiltration of ground water may be calculated based on the deviation of soil water potential from water potential at field capacity, which equals the amount of energy available for water ascent (Pietsch et al., 2003). Soil water potential consists of two different forces, which counter-act on vertical ground water movement. The first,

gravitation, acts downwards, and the second, soil matric potential, which is given by the deviation from the matric potential at field capacity, is directed upwards. The sum of both forces drives water infiltration from the ground water table into the rooting zone. The amount of water ascent per day depends on soil hydraulic conductivity. The calculation (see Pietsch, 2003) starts from the deviation of water potential from field capacity ($\Delta\Psi$) given by

$$\Delta\Psi = \frac{\mu_{fc} - \mu_{act}}{\overline{V_w}}, \tag{19.15}$$

whereby μ_{fc} is the chemical potential of soil water at field capacity, μ_{act} is the chemical potential of soil water at the actual water content and $\overline{V_w}$ is the partial molal volume of water which is always close to 1.8 x $10^{-5}\,m^3\,mol^{-1}$. Since water has no net charge, the electrical term of the chemical potential can be neglected, thus leaving μ_{fc} and μ_{act} as

$$\mu_{fc} = \mu^* - \overline{V_w}\Pi_{fc} + \overline{V_w}P_{fc} + mgh_1, \tag{19.16}$$

$$\mu_{act} = \mu^* - \overline{V_w}\Pi_{act} + \overline{V_w}P_{act} + mgh_2, \tag{19.17}$$

where μ^* is the arbitrary reference potential, Π_{fc} and Π_{act} are the matric potential at field capacity and actual soil water content, P_{fc} and P_{act} are the hydrostatic pressure difference between atmosphere and soil water content at field capacity and at actual soil water content, m is the molar mass of water, g is the rate of gravitational acceleration and h_1 and h_2 are the potential heights of soil water, which will be explained in Eq. (19.21).

The soil matric potential is calculated from soil texture data using an equation fitted by Brooks and Corey (1964) in a simplified form as used by Clapp and Hornberger (1978),

$$\Pi_{act} = \Pi_{sat} \cdot \left(\frac{\Theta_{act}}{\Theta_{sat}}\right)^{-b}, \tag{19.18}$$

with Π_{act} and Π_{sat} as the matric potential, Θ_{act} and Θ_{sat} as the volumetric water content at actual and saturation soil water content, respectively, and b the slope of the retention curve (see Cosby et al., 1984).

By substituting Eqs. (19.16) and (19.17) into Eq. (19.15) the reference potential and the hydrostatic pressure terms are cancelled out, thereby explicitly excluding differences in hydrostatic pressure as possible cause of water ascent. This leaves Eq. (19.15) in the form

$$\Delta\Psi = \frac{\overline{V_w}(-\Pi_{fc} + \Pi_{act}) + mg(h_1 - h_2)}{\overline{V_w}}. \tag{19.19}$$

Since mass equals density multiplied by volume, the partial molal volume can be removed and Eq. (19.19) can be rewritten as

$$\Delta\Psi = (-\Pi_{fc} + \Pi_{act}) + \rho_w g(h_1 - h_2), \tag{19.20}$$

where ρ_w is the density of soil water and is set to $1,000\,kg\,m^{-3}$, as an approximation over the possible temperature range of soil water (1,000 at 4°C and less than 0.5% deviation between −30 and +30°C).

When calculating the gravitational force, the difference in potential soil water height needs to be defined. The potential height is the increase in potential energy in accordance with vertical water ascent, which occurs when the soil water content is below field capacity. The calculation is based on the deviation of the actual soil water content from the soil water content at field capacity. Soil water mass is converted into soil water volume using the approximation for ρ_w given above, which changes the units from [kg m^{-2}] to [m^3 m^{-2}] or simply [m]. The division of this number by the porosity at field capacity gives the potential height of soil water. Formally $h_1 - h_2$ is then defined by

$$(h_1 - h_2) = \frac{sw_{fc} - sw_{act}}{1000 \cdot \Theta_{fc}}, \tag{19.21}$$

where sw_{act} and sw_{fc} are the actual soil water content and the soil water content at field capacity [m], respectively, and Θ_{fc} is the volumetric water content at field capacity, which equals the non drainable porosity. The actual amount of ground water (gw_{in}) entering the rooting zone per unit time is given by

$$gw_{in} = K \cdot \Delta\Psi \tag{19.22}$$

with $\Delta\Psi$ indicating the overall force acting on ground water as defined in Eqs. (19.20) and (19.21) and where K is the soil hydraulic conductivity coefficient, calculated from the soil texture and actual soil water content according to Saxton et al. (1986):

$$K = 2.778 \cdot 10^{-6} \cdot \exp\left(a_0 + a_1 \cdot \%s + \frac{a_2 + a_3 \cdot \%s + a_4 \cdot \%c + a_5 \cdot \%c^2}{\Theta_{act}}\right), \quad (19.23)$$

whereby $\%s$ and $\%c$ give the percentages of sand and clay, a_0–a_5 are the coefficients calculated via multiple nonlinear regression techniques (see Saxton et al., 1986), and Θ_{act} is the actual volumetric water content.

3. Mortality

Studies on the temporal development of mortality rates in production forests revealed that mortality rate follows a U- or J-shape versus stand age (see e.g. Harcomb, 1987; Peterken, 1996; Lorimer et al., 2001; Monserud and Sterba, 2001). Under undisturbed conditions mortality rate decreases from regeneration via juvenescence and reaches a minimum during the optimum phase of ecosystem development. Mortality increases again, towards the old growth and breakdown stages. Under undisturbed conditions, the U-shaped development of mortality can be assumed (Pietsch and Hasenauer, 2006). Since the death of old biomass-rich individuals creates space for regeneration, the two ends of the "U" – shape will overlap. Hence, a trajectory consisting of two individually scaled half-ellipses can be used to describe the temporal evolution of the mortality rate (Fig. 19.2). Formally, both ellipses are given by

$$\frac{(x - c_x)^2}{a^2} + \frac{(y - c_y)^2}{b^2} = 1, \quad (19.24)$$

where c_x, c_y are the x- and y coordinates of the centre of the respective ellipse, a and b are the two semi-axes, x is time and y is the mortality rate. Solving this quadratic equation for y gives

$$y = c_y \pm \frac{b}{a}\sqrt{a^2 - x^2 + 2xc_x - c_x^2}. \quad (19.25)$$

The semi-axes a, b and the center coordinates c_x, c_y of the ellipse can be expressed as

$$a = c_x = \frac{T}{2}, \quad (19.26)$$

$$b = \frac{mort_{max} - mort_{min}}{2}, \quad (19.27)$$

$$c_y = b + mort_{min} = \frac{mort_{max} + mort_{min}}{2}, \quad (19.28)$$

where T is the length of the low or high mortality phase, and $mort_{max}$ and $mort_{min}$ are the maximum and minimum m ortality rates. Substituting the Eqs. (19.26), (19.27) and (19.28) into Eq. (19.25) results in

$$y = \frac{mort_{max} + mort_{min}}{2} \pm \frac{mort_{max} - mort_{min}}{T} \cdot \sqrt{T \cdot x - x^2}. \quad (19.29)$$

In Eq. (19.29) the first right hand term is the mean annual mortality rate. The second right hand term governs the changes along the mortality cycle. Subtraction gives the trajectory of the low mortality phase and addition gives the trajectory of the high mortality phase (Fig. 19.2). The parameters $mort_{max}$, $mort_{min}$ and T vary by species and site and climate conditions and may be set for each stand separately or generalized for a watershed or region.

C. Model Parameters

The parameters of complex large-scale ecosystem models define key properties of the modeled ecosystem. Model parameters include (i) allometric parameters, regulating the allocation of carbon assimilated via photosynthesis to the different root and shoot compartments, (ii) turnover and mortality parameters, describing the portions of the plant pools that are either replaced each year or removed through plant death, (iii) N/C

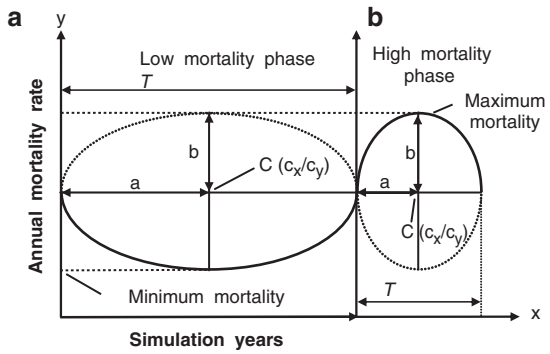

Fig. 19.2. The trajectory of mortality (bold line) along the lower half (**a**) and upper half (**b**) of two individual ellipses. The x and y axes denote time and mortality rate, respectively. $C(c_x/c_y)$ are the coordinates of the centers of the ellipses, *a* and *b* are the two half-axes, *T* is the length of each mortality cycle along the half-ellipses (Pietsch and Hasenauer, 2006)

ratios, which define nutrient requirements for new growth, photosynthetic capacity, plant respiration rates and litter quality, (iv) percentages of lignin, shielded and unshielded cellulose, and labile material in fine roots, leaves and dead wood, controlling litter recalcitrance and influencing decomposition rates, (v) morphological parameters, which define the distribution of LAI at the leaf and canopy level, (vi) single parameters that define water interception, canopy radiation absorption and the time span of transfer growth and litter fall, as proportions of the growing season and (vii) ecophysiological parameters, controlling rates and limitations of leaf conductance for water and carbon dioxide. Ecophysiological parameters are a special case because they follow fast dynamics and their values have to be chosen according to the temporal resolution of the model implementation (see Section III.E).

According to the type of model application, the values of the parameters reflect either general plant functional types (biomes) such as evergreen needle leaf (ENF), deciduous needle leaf (DNF), deciduous broadleaf (DBF), evergreen broadleaf (EBF), C_3 grass, etc. or they represent specific ecosystems dominated by a single species (e.g. beech or spruce forests, etc.) or an ecosystem specific assembly of species (e.g. arid grasslands, temperate pastures and meadows or tropical savannas). The restriction to certain biomes is logical for assessing the fluxes of energy, water, carbon and nitrogen on a continental or global scale. If the same information is required at the regional to local scale, specific ecosystem parameters may be needed and useful. This is especially important in large parts of Europe where historic land use as well a sylvicultural management practices strongly have affected the species distribution and the structure of central European forests (Spiecker et al., 2004). Different species have different impacts on site quality due to species-specific differences in litter production, chemistry and decomposition rates contributing to the quantity of nutrients cycled between vegetation and soil (Schlesinger, 1997; Finzi and Schlesinger, 2002).

For Central Europe, parameter sets exist for grasslands, meadows and pastures (Pietsch and Hasenauer, 2003) and the major forest types like Common beech, Sessile/pedunculate oak, European larch, Cembran pine, Scots pine and Norway spruce forests, the latter represented by two different parameter sets to cover the different ecophysiology of highland and lowland spruce variants (Pietsch et al., 2005). An example for biome specific parameter sets is given in White et al. (2000).

D. Model Drivers

Model drivers may be distinguished as (i) static, (ii) slow or (ii) rapidly changing variables. Static input variables are elevation, slope and aspect as well as soil depth and soil texture. Static model drivers are site-specific properties that do not change during a simulation. Soil depth and soil texture determine the soil water outflow, retention and evaporation and influence plant water uptake. If not measured they may be interpolated from surrounding sites using Kriging techniques (Petritsch and Hasenauer, 2007). Slope and aspect define the exposition that is important for solar radiation input. Elevation determines the atmospheric pressure and thereby influences the partial pressures of atmospheric CO_2 and water vapor. A lower partial pressure of CO_2 decreases the amount of external CO_2-molecules and hence the thermodynamic gradient between intracellular CO_2 and external atmospheric CO_2, i.e. the driving force for CO_2 uptake. Exactly the opposite is evident for H_2O because the transport of water moves in the opposite direction as CO_2. While the intracellular amount of water will always be close to 56 mol l^{-1}, the amount of

external atmospheric water molecules is reduced under lower atmospheric pressures. Slope aspect and elevation may be known from on site determination, or it may be taken from digital elevation maps.

Slow dynamic model drivers change from year to year. A typical example is the nitrogen deposition rate, which depends on regional topography, wind direction and the precipitation regime. The levels of this parameter have increased substantially since pre-industrial times. Historical nitrogen deposition is published by Holland et al. (1999), or for Central Europe by Ulrich and Williot (1993). Present day nitrogen deposition data for Central Europe is available from regional interpolations using data from permanent field stations (e.g. Schneider, 1998). Another slow model driver is the increase in atmospheric CO_2 concentration, which is a global property and does not change from plot to plot. Historical records of atmospheric CO_2-concentration are available from ice core measurements (Petit et al., 1997, 1999; Etheridge et al., 1996) and from measurements in recent decades (Keeling et al., 1989).

Model inputs with fast dynamics are meteorological variables, such as temperature, precipitation, radiation and vapor pressure deficit, which change within less than a daily time step. These data may be available from measurements, or may be extrapolated from the nearest climate station (Thornton et al., 2000). Another option is provided by interpolation of data from multiple climate stations using Gaussian filters (Hasenauer et al., 2003) or Kriging methods (Petritsch and Hasenauer, 2007). Sometimes meteorological input data is generated using statistical methods, such as the Markov chain approach (Richardson and Wright, 1984; Racsko et al., 1991; Semenov et al., 1998) or dynamic methods such as atmospheric circulation models (Tiedtke, 1989; Collins et al., 2002).

E. Temporal Model Resolution

Model drivers induce fluxes amongst the pools by changing the size of each pool. The length of the time step of the recursion defines the temporal resolution within the model. For large scale models it may range from one second (ORCHIDEE, Krinner et al., 2005) to one month (TEM, Melillo et al., 1993), typically it is one day (LPJ, Sitch et al., 2003; Biome-BGC, Thornton, 1998; MC1, Bachelet et al., 2001). Regardless of the chosen time step the model drivers with fast dynamics have to be adapted to fit the time step. For meteorological drivers this adaptation is achieved by averaging the values over the time step that is implemented in the model. For a daily time step e.g., day time air temperature (t_{day}), which affects leaf temperature during photosynthesis, may be estimated from the daily minimum and maximum air temperature (t_{min}, t_{max}) as

$$t_{day} = 0.45 \cdot \left(t_{max} - \frac{t_{min} - t_{max}}{2} \right) + \frac{t_{min} - t_{max}}{2}. \tag{19.30}$$

Other meteorological model drivers may be fitted to a daily time step by averaging the values over the length of the daylight period. The length of the daylight period may be calculated from daily earth-sun geometry and the position on earth (Carbone, 2007). The amount of daily photosynthetic carbon assimilation is then calculated using t_{day} in Eqs. (19.6)–(19.10) for Rubisco limited photosynthesis or mean daytime radiation in Eq. (19.13) for electron transport limited photosynthesis. The minimum of both (see Eq. 19.3) is then multiplied with the length of the daylight period in order to give an estimate for photosynthetic carbon assimilation over the modeled time step (e.g. 1 day). Note that the average output value of nonlinear functions (e.g. photosynthesis rate) may not match the output value achieved by using average values of variables (e.g. for radiation or temperature) in nonlinear equations. For a daily time step, the calculated value may be lower or higher versus the average output value of the non linear function. It is important to check that the averaging procedure does not lead to differences in the mean values of the nonlinear function if calculated over multiple simulation steps (see e.g. Fig. 19.8).

A similar averaging approach is applied to the ecophysiological parameters controlling stomatal conductance (g) to water vapor and CO_2. Stomatal conductance has an upper limit (g_{max}) which is down-regulated to actual stomatal conductance (g_{act}) by environmental factors, such as leaf water

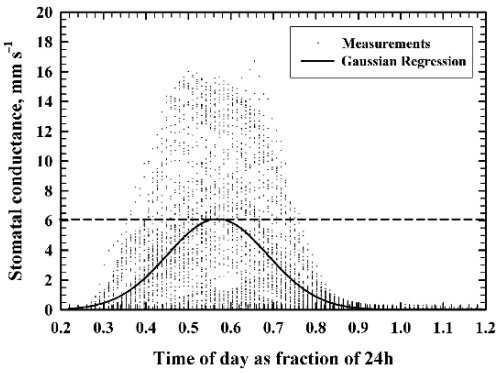

Fig. 19.3. Stomatal conductance of Common beech in Kreisbach, Austria. Measurements were performed every 15 min throughout the growing season 1999. The maximum of the daily average stomatal conductance used in a model with a daily time step results from the peak of a Gaussian regression as indicated by the dashed line. For Common beech the value of the maximum of daily average stomatal conductance equals 6 mm s^{-1}

potential (Ψ), previous minimum air temperature, daytime vapor pressure deficit (vpd) and radiation (PHAR):

$$g_{act} = g_{max} \cdot m_{tmin} \cdot m_{vpd} \cdot m_{\Psi} \cdot m_{PHAR}. \quad (19.31)$$

The variables m_x are multipliers with values between 0 and 1, which are used to reduce g_{max} to g_{act}. Since radiation and vapor pressure deficit are mean values for a given time step the parameter g_{max} also needs to be averaged for the time step. Fig. 19.3 illustrates this averaging step for daily g_{max} of Common beech as previously outlined.

IV. Model Application

In this section the principles of model application within different spatial and temporal scales will be presented as follows: (i) precursor modeling steps to model a current ecosystem's behavior, (ii) tests for model sensitivity, (iii) how a large scale ecosystem modeling may be validated, and (iv) how model dynamics may be assessed.

A. Application Procedure

Model applications often begin with the assumption that undisturbed conditions exist as they would within a virgin ecosystem (Pietsch and Hasenauer, 2002). This initial state assumes that human management activities are absent and the ecosystem has had sufficient time to reach its dynamic equilibrium. In models the virgin ecosystem conditions are achieved by so called self initialization procedures. During self initialization the model is run until the running average of each model output approach steady state. The time scale for averaging is the length of one complete mortality cycle. In model implementations, the possibly infinite time needed to reach the steady state is shortcut by comparing the averages of soil carbon content. Soil carbon content is the last among the pools reach a steady state, and self initialization is terminated when the average soil carbon content differs by less than 0.5 g C m^{-2} between two successive mortality cycles.

The results of the self initialization procedure need to be corrected for possible degradation effects due to changes in land use and ecosystem management (Pietsch and Hasenauer, 2002). Conceptually, this step is essential, as historic land management may have led to a decline in nutrient status and soil fertility (Mayer and Ott, 1991; Ott et al., 1997). Therefore, scenarios of historical land use are assumed, and simulated, as part of the model initialization process (Pietsch et al., 2005) prior to the actual simulation run. A typical historical land use scenario for Central Europe is the assumption that repeated clear cuts have occurred at intervals of 20 (coppice systems), 100 (Norway spruce ecosystems) or 200 years (Cembran pine ecosystems). Fig. 19.4 depicts the conceptual outline and the corresponding modeling steps.

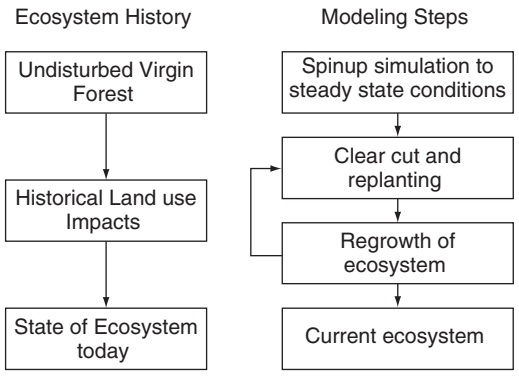

Fig. 19.4. The historical development of a typical ecosystem in Central Europe from undisturbed virgin forest conditions, via intensive historical land use to the state of the ecosystem today, and the modeling steps mimicking this development (Pietsch et al., 2005)

B. Sensitivity

The sensitivity of a large scale ecosystem model is a property, which describes the range of model predictions caused by variations in model parameters and model drivers. It may be assessed by a partial, full or complete sensitivity analysis.

In the partial sensitivity analysis single model parameters are tested, for example, by comparing with field observations. The resulting relative variation of model outputs (e.g. NPP, LAI, biomass carbon storage, etc.) is then related to the relative variation of the chosen input parameter. An evident constraint of this approach is that the sensitivity of the model with respect to a single parameter varies depending on the values of other parameters and site and climate conditions. For example, in tropical forests, generally stocking on deep clayey soils and frequent rainfall throughout the year, the parameters determining stomatal conductance (soil water potential and atmospheric VPD) have a low impact on the stomatal conductance and on the model performance. In forests stocking on shallow sandy soils with extended periods without rainfall, stomatal conductance and other model outputs will be highly sensitive to these parameters. In alpine forest ecosystems, the low minimum temperatures may become the key controlling parameter for stomatal conductance (Pietsch and Hasenauer, 2005b). Model sensitivity to this parameter may mask the sensitivity to soil water potential or VPD; therefore, partial sensitivity analysis is a useful tool when (i) the ecosystem type is well defined, (ii) the range of site conditions is known and (iii) the temporal variation in model drivers can be estimated. Partial sensitivity analysis may also be used in estimating the parameters of processes added to the model algorithm. This assumes that all other parameters are defined or derived from previously validated model runs. In such cases, new parameters are varied along a grid of reasonable values in order to select the values with the best fit compared to real observations (Pietsch and Hasenauer, 2006).

Full sensitivity analysis uses sets of randomly selected model parameters. Each set of parameters is used for model simulations across the estimated range in site and climate conditions using Monte Carlo methods. Full sensitivity analysis is useful if the ecosystem is poorly defined. It may be used to assess the type of ecosystem which occurs under certain site-specific and climatic conditions. This approach may be considered as an optimization procedure; however, the results have to be interpreted carefully since nonlinear systems such as ecosystem models may exhibit several solutions. Note that not all ecosystems which could occur under given site and climate conditions, are the result of evolutionary, human and/or random impacts and constraints.

Complete sensitivity analysis is done by varying model parameters, site conditions and model drivers. This approach is the most thorough test of model sensitivity and allows one to theoretically explore which ecosystems may emerge under certain physical, site-specific and climate constraints.

C. Validation

A large-scale ecosystem model together with its parameters resemble a formalized, scientific hypothesis of observable real-world phenomena. Since the work of Popper (1935) it has become widely accepted that scientific hypotheses must be falsifiable. A hypothesis that cannot be falsified by observations is a belief, and as such it is not a scientific result. With respect to large scale ecosystem models, falsification is accomplished by comparing predictions versus field observations and error assessment.

Model errors have several reasons. Firstly, ecosystem models always represent an abstraction and simplification of reality; they can not take all ecosystem processes into consideration. Secondly, the temporal resolution of the model (see Section III.E) may vary between one second (ORCHIDEE, Krinner et al., 2005), 1 day (LPJ, Sitch et al., 2003; Biome-BGC, Thornton, 1998; MC1, Bachelet et al., 2001) and one month (TEM, Melillo et al., 1995). Additionally, the accuracy of field observations contributes to model errors. All instruments and methods exhibit uncertainties in measurement. Lastly, the lack of complete information about the status of an ecosystem when model application begins (see Section III.A) is likely one of the most important uncertainties in model application.

Within model validation, criteria are necessary to help with the assessment of the accuracy,

precision and bias of predictions. Model accuracy is described by the mean error and is calculated as the difference between the mean of predictions and the mean of observations. Precision is the variation of the errors versus the mean error. A model is biased if the predicted mean is significantly different from the observed mean. One option to determine model error ranges and their limits is to calculate the confidence, prediction and tolerance intervals of predictions as described by Reynolds (1984). The confidence interval CI for the mean of the differences can be used to evaluate discrepancies between the observed and estimated mean. The prediction interval PI can be interpreted as the range of the differences among predictions versus observations. The tolerance interval TI provides the limit that contains a specified portion (e.g. 95%) of the distribution of the differences when the model is used repeatedly. This type of error assessment requires normal distribution of model errors.

D. Dynamic Model Behavior

Large-scale ecosystem models describe the dynamics of physical, chemical and biological processes within ecosystems. Classical methods of model validation (see Section IV.C) capture static aspects of the model but fail to assess model dynamics. Like ecosystems themselves, ecosystem models may exhibit stable, instable or chaotic dynamics (Pietsch and Hasenauer, 2005a, 2006). The assessment of the type of prevailing model behavior may be done using methods from ergodic theory (Eckmann and Ruelle, 1985). The word ergodic is a combination of the Greek words for work (ergon) and path (odos) and was first used in statistical mechanics, when Boltzmann (1877) used probability to define entropy. Later, Poincaré (1982) studied the stability of the dynamics of planetary orbits and found that consecutive orbits differed in length and shape (see Fig. 19.5a), i.e. where not periodic but quasi-periodic. The most important finding by Poincaré was that the behavior of a dynamic system may be analyzed by (i) inserting a single plane orthogonal to the flow of the trajectories (Fig. 19.5b), and (ii) by looking at the return of the system's trajectory within the plane after traveling a full quasi period (Fig. 19.5c). He suggested that the orbital dynamics are stable when the intersection points stay within a limited area of the plane and that the orbital dynamics have to be considered as unstable if they leave this area. This approach to analyze dynamic systems is called a Poincaré map, which contains all the information to characterize the dynamics of the system, but only provides a one dimensional time series (Ruelle, 1995). Ruelle (1978) proposed that the Poincaré map provides the contour or silhouette of the space attracting the system and suggested that if one looks at this silhouette from different directions a multidimensional picture of system behavior will emerge. He reached this effect by grouping consecutive points of the Poincaré map in n-tuples, i.e. ordered sets of pairs (2-tuples), triplets (3-tuples), etc. The mathematical proof of Ruelle's assumption was provided by Takens (1981). The n-tuples created using the Ruelle-Takens transformation may be drawn in an n-dimensional graph depicting the full dynamics of the system, where n denotes the degrees of freedom of the system and is equal to the number of dynamic system drivers minus one. Such graphs are called attractors and provide an opportunity to visually distinguish between stable and unstable dynamics.

The Poincaré map and the Ruelle-Takens transformation may also by applied to the outputs of large scale ecosystem models, because the models are driven by daily weather values which resemble climate. Climate is a quasi periodic system (Broer et al., 2002), because it is similar from year to year, but always a little different in the temperature and precipitation profiles which is responsible for the different lengths of successive growing seasons. The quasi periodicity of model inputs is transferred to the model outputs. For model outputs the length of one quasi period may be determined as the time span between the start of the growing season to the start of the next growing season. Fig. 19.5d provides an example of an attractor reconstructed from modeled NPP of 22 Cembran pine stands from the time of planting (between 1748 and 1932) up to the year 1998. The attractor is embedded in a three-dimensional graph because three out of seven dynamic model drivers (minimum temperature, maximum temperature, precipitation, PHAR, VPD, CO_2 concentration and nitrogen deposition; see Section III.D) are calculated from the others: PHAR

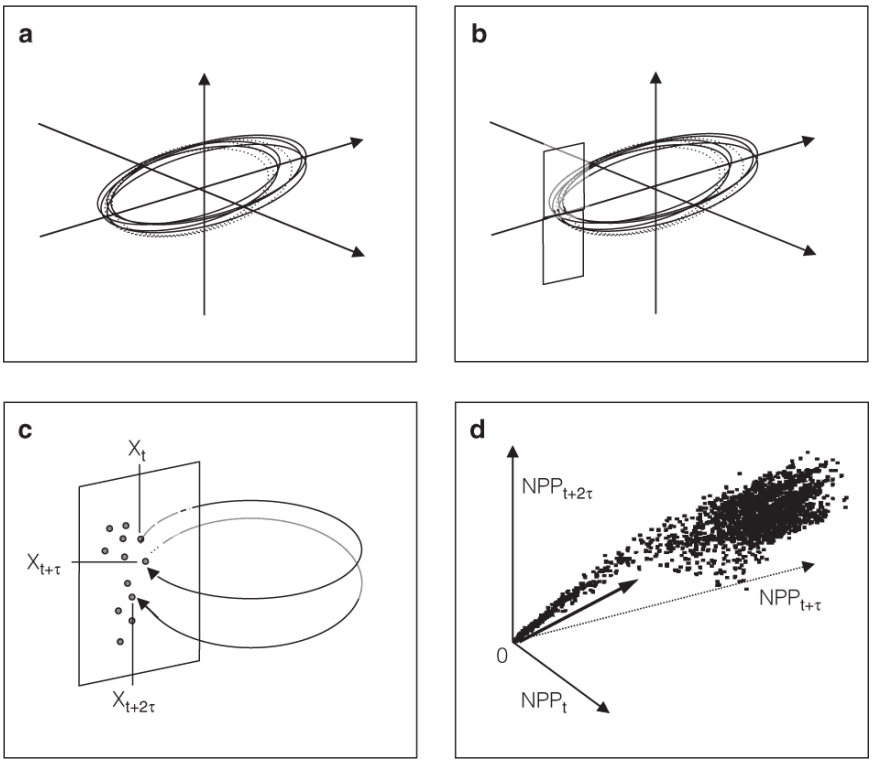

Fig. 19.5. **a**: Quasi periodic motion of a planet in space. The cycle length τ varies among the individual turns. **b**: Placing a plane at one position of the orbit and plotting the points in the plane. **c**: The points where the systems trajectories cross the plane give the Poincaré map of the system, i.e. the series of points X_t, $X_{t+\tau}$, $X_{t+2\tau}$, ... The points of the Poincaré map can be seen as a one dimensional time series. **d**: A Ruelle-Takens transformation groups consecutive points of the Poincaré map into an ordered sets of n-tuples $\{(X_t, X_{t+\tau}, \ldots X_{t+n\tau}), (X_{t+\tau}, X_{t+2\tau} X_{t+(n+1)\tau}), \ldots\}$ representing the attractor of system behavior. The attractor shown here was reconstructed from NPP predictions for 22 Cembran pine plots planted between 1,748 and 1,932 close to Murau, Austria. The attractor was embedded in a three-dimensional system since the simulation was run with four independent model drivers resulting in three degrees of freedom (see text). The time of planting (lowest NPP values) resembles the source of the NPP attractor. The arrow indicates the direction of stand development over time. The attraction basin enlarges at higher NPP values when canopy closure increases the competition for resources (Pietsch and Hasenauer, 2005a)

and VPD are calculated from (i) minimum and (ii) maximum temperature and (iii) precipitation (Hasenauer et al., 2003) and the increase in nitrogen deposition is derived from (iv) the increase in CO_2 concentration. This results in four independent model drivers, three degrees of freedom or a three-dimensional system for embedding the attractor. A detailed description for the application of this attractor reconstruction procedure is given in Pietsch and Hasenauer (2005a).

Typical examples of ecosystem and ecosystem model behavior are sources, sinks, limit cycles, saddles or riddled basins. Large-scale ecosystem models are stable when the attractor configuration is a source, a sink or a limit cycle. In such situations model behavior is fully deterministic. Model behavior is unstable when saddle-like attractor configurations occur, as the model becomes very sensitive to small variations in early conditions of simulation and diverging final results cannot be predicted, but must be explained only after the simulation run. Examples of such model behavior come from studies on lake eutrophication in which the ecosystem exhibits a sudden shift from standard dynamics to algal blooms (Scheffer et al., 2001). Such model behavior is called post-deterministic. Model behavior must be classified as chaotic when retrospective explanation of diverging model results is not possible due to statistically indistinguishable earlier conditions. In such cases model application is meaningless.

V. Examples of Model Application

This section presents three modeling examples referring to the application procedures outlined in Section IV. The first example will deal with virgin forest conditions, the second example will address the necessity of ecosystem specific parameter choice for model validation and the third example will demonstrate the assessment of model dynamics.

A. Application to Virgin Forests

Among real world ecosystems, virgin forests resemble the best approximation of natural conditions. Natural conditions refers to (i) the absence of human exploitation of forest resources such as timber, litter, fruits, resin or water and (ii) the absence of silvopastoral-, pathogen- or game-management practices. Here we present a model application example of the central European virgin forest reserve Rothwald, a first-category IUCN wilderness area with a documented absence of logging and forest management for more than 700 years (Pietsch and Hasenauer, 2006). Rothwald is one of the last virgin forest areas in the Alps and covers approximately 250 ha of unmanaged forest with different successional stages from regeneration to optimal and breakdown phases. In virgin forests such as Rothwald a mosaic of different stages shifts over time, but the abundance of all stages remains constant if the region is large enough (Heinselman, 1973). The 'mosaic cycle' concept of ecosystems (Remmert, 1991) assumes the maintenance of an overall steady state at the landscape level with local disequilibria due to vegetation dynamics. Rothwald resembles such a mosaic cycle and provides an excellent test case for the accuracy of the self-initialization procedure of complex large scale ecosystem models.

We first collected data on stem, soil and necromass carbon and nitrogen content from 18 permanent field plots across all successional stages. Next, we ran standard model self-initialization using a constant annual mortality rate of living biomass. Model predictions for the 18 sites, on average exhibited an overestimation of ecosystem carbon content of up to 400% (Pietsch and Hasenauer, 2006). The inconsistency of model results was due to the assumption of constant mortality. When mortality is kept constant, the ecosystem remains a net carbon sink until a steady state is established at ecosystem carbon saturation; however, in the real world an ecosystem exhibits a life cycle from regeneration via juvenescence to optimal growth, old growth and breakdown. During the early phases of an ecosystem's life cycle concurrence among individuals is high, which results in the death of individuals not fit enough to survive the competition with stronger individuals. In such situations mortality is high and the number of individuals declines. This competition induced mortality rate decreases until the trees reach the physiologic limitation of their life cycle. The remaining big trees die and biomass mortality is high. The open space will then be covered by regeneration and the next successional cycle begins.

Based on these successional principles a dynamic mortality routine as outlined in Fig. 19.2 may be used. For estimating the parameters of minimum and maximum annual mortality rate of vegetation biomass partial sensitivity analyses were used by testing minimum annual mortality rates between 0.5% and 2.5% and maximum annual mortality rates between 0.5% and 15%. The results of this calibration procedure were 0.9% minimum and 6% maximum annual mortality rate (Pietsch and Hasenauer, 2006), and using these settings the model delivered unbiased results for the mosaic cycle represented by the virgin forest reserve Rothwald (Fig. 19.6).

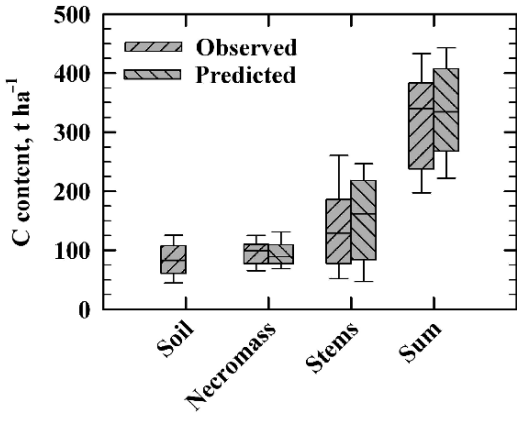

Fig. 19.6. Predicted compared to observed C content of soil, necromass, stems and their sum using the dynamic mortality model during self-initialization for the virgin forest reserve Rothwald in Austria. The boxes represent the 25% and 75% percentiles and the whiskers show the 10% and 90% percentiles of predictions and observations (Pietsch and Hasenauer, 2006)

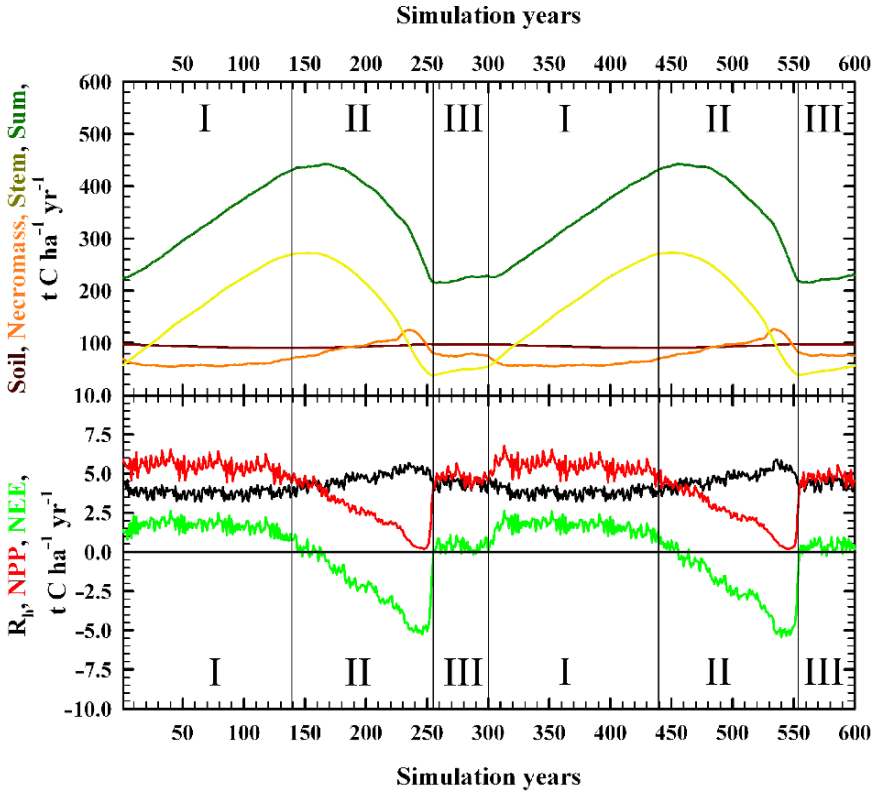

Fig. 19.7. Modeled pools and fluxes for the virgin forest reserve Rothwald using model parameters for Common beech forests. Upper graph: Comparison of the temporal development of modeled soil, necromass, stem and total ecosystem carbon content for 600 simulation years at landscape level steady state. Lower graph: Corresponding annual C fluxes from heterotrophic respiration (R_h), net primary production (NPP) and net ecosystem exchange (NEE). I – optimum phase; II – breakdown/regeneration phase; III – juvenescence (Pietsch and Hasenauer, 2006). See also Color Plates, Fig. 5

Ecosystems exhibit periods in which they act as a net carbon sink (optimum phase), as carbon neutral (stationary phases with no net carbon exchange – old growth, juvenescence) and as a net carbon source (breakdown, regeneration). Such source-sink transitions are a part of natural ecosystem dynamics and they restrict complex large scale ecosystem models to the steady state at the landscape level. Fig. 19.7 presents an example of the development of carbon pools and ecosystem fluxes for two life cycles of one of the plots in the virgin forest Rothwald.

Figure 19.7 shows the simulation of the carbon dynamics of a virgin forest including periods in which the system acts as a C-source and a C-sink. The amount of carbon assimilated during the optimum phase of growth is released during breakdown and regeneration phases. Over the complete life cycle of the virgin forest the net rate of carbon sequestration equals zero. This is an important result given that virgin forests are considered as the optimal stage of ecosystem carbon storage and are often seen as the reference for managed forests!

Although the goal of this study was to test and adjust the self initialization procedure as it is used within large scale ecosystem modeling, we demonstrated also the C sink and C source behavior of old growth forests. Regular timber extraction helps to keep a forest in the optimum phase of growth and at a high level of net ecosystem carbon sequestration via photosynthetic carbon assimilation. This is an issue of increasing importance in the context of climate change and mitigation measures.

B. Assessing Ecosystem Specific Model Parameters

Applications of ecosystem models at the continental or global scale use parameter sets capturing broad ecophysiological characteristics of plant functional types or biomes, such as evergreen needle leaf forests, deciduous broadleaf forests, temperate grasslands, tropical savannas, etc. One constraint of this approach is that in Europe as well as in many other parts of the world, historic land use and ecosystem management practices strongly affected ecosystem structure and species composition (Spiecker et al., 2004). Additionally, plant functional types restrict the integration of species-specific growth responses induced by forest management practices (e.g. tending, thinning, etc.). Such interventions change the biomass density within the forest and the growth of the remaining biomass is strongly sensitive to tree species (Assmann, 1970).

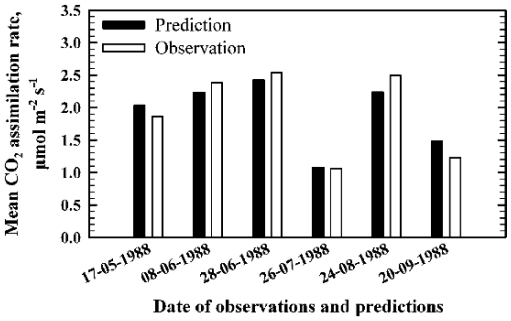

Fig. 19.8. Predicted and observed carbon assimilation rates of shade leaves of Common beech in Hochbuch, Vienna Woods, Austria. Assimilation rate is given on a m^2 leaf area basis. Observed values reflect the mean value of half-hourly measurements taken during the daylight period of the respective day (Pietsch and Hasenauer, 2002)

Within large scale ecosystem models, the type of ecosystem is defined by model parameters. Accordingly, a tree species may be defined by obtaining species-specific model parameters from the literature and/or from in-depth research sites. This information allows a "tuning" or "calibration" process for a given tree species. Typical examples of field observations and model predictions by tree species are given for daily mean CO_2 assimilation (Fig. 19.8), stomatal conductance (Fig. 19.9), transpiration and soil water content (Fig. 19.10). In our efforts to produce a species specific BGC model we established parameter sets for Common beech (*Fagus sylvatica*), pedunculate/sessile oak (*Quercus robur/petraea agg.*), European larch (*Larix decidua*), Scots pine (*Pinus sylvestris*), Cembran pine (*Pinus cembra*) and Norway spruce (*Picea abies*) forest ecosystems in central Europe. For Norway spruce, two different parameter sets were necessary to cover the physiological differences between highland (>1,000 m a.s.l.) and lowland (<1,000 m a.s.l.) variants. For details and the full set of parameters by species we refer to Pietsch et al. (2005).

Once such parameter set is established with data from intensive research plots in combination with published literature, the species specific model performance needs to be tested across the growing conditions of a species. The key is that the parameters defined using limited data need to produce unbiased and consistent results in large scale applications. Available data for this type of validation typically come from forest inventories (Fig. 19.11).

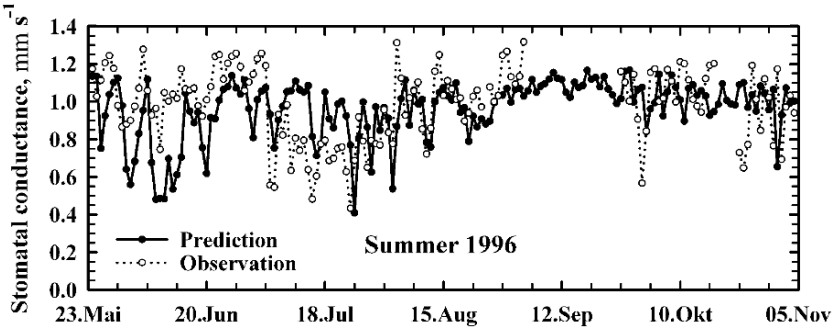

Fig. 19.9. Predicted and observed daily mean stomatal conductance of Cembran pine on Mt. Patscherkofel, Austria, during the summer 1996 (Pietsch and Hasenauer, 2005b)

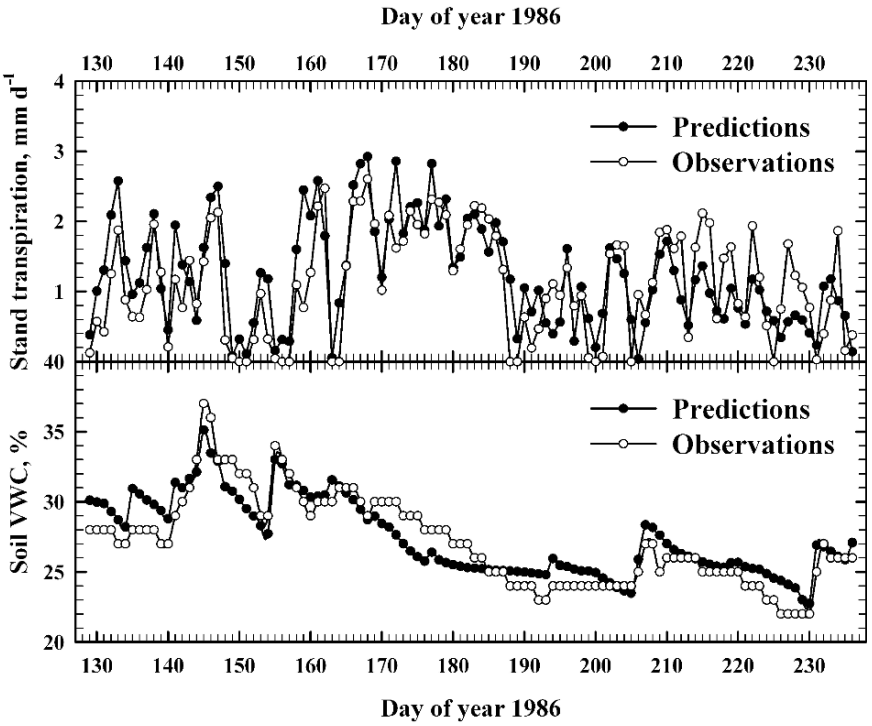

Fig. 19.10. Predicted and observed daily stand transpiration and soil volumetric water content (VWC) of a Norway spruce stand in Zebrakovsky creek, Czech Republic (Pietsch and Hasenauer, 2002)

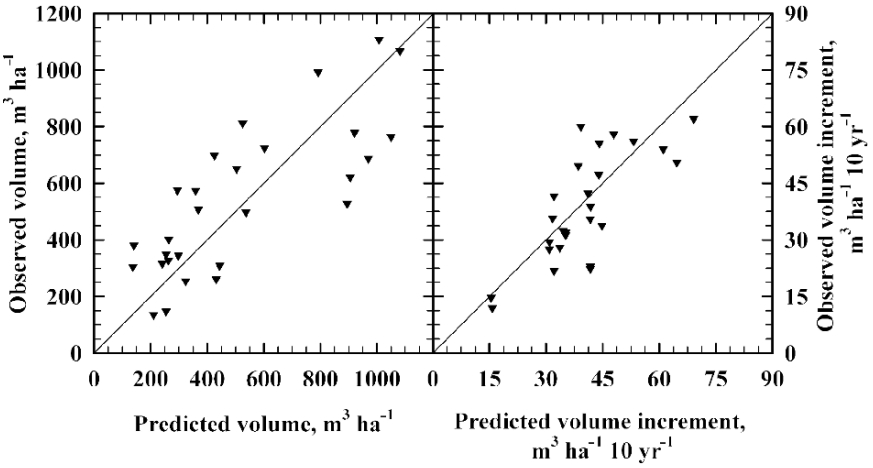

Fig. 19.11. Predicted and observed volume (*left*) and 10-year volume increment for 24 lowland stands of Norway spruce in Austria (Pietsch et al., 2005)

C. Assessing Model Dynamics

Model dynamics such as real world ecosystem dynamics may exhibit stable and unstable phases. The attractor represents system dynamics (see Section IV.D). This section presents an example of stable ecosystem model behavior and explains the importance of analyzing the attractor of model dynamics. For an example of unstable model behavior we refer to Pietsch and Hasenauer (2005a).

The attractor shown in Fig. 19.12a represents the dynamics of modeled Net Ecosystem carbon Exchange (NEE) of the virgin forest successional cycle (optimum, old growth, breakdown, regeneration and adolescence phases) using the site conditions of 18 established research plots. Fig. 19.12b shows the same for one single plot and one development cycle in order to demonstrate that the attractor represents a limit cycle (i.e. a stable configuration of ecosystem model behavior). The attractor of NEE is embedded in a two dimensional graph, since in this application (i) VPD and (ii) PHAR were calculated from temperature and precipitation (Hasenauer et al., 2003) and (iii) CO_2-concentration and N-deposition were kept constant throughout the simulation. This reduced the number of seven independent dynamic model drivers to three, i.e. daily minimum temperature, maximum temperature and precipitation. Three independent model drivers result in two degrees of freedom and a two dimensional attractor of model dynamics (see Section IV.D).

In the attractor of virgin forest dynamics, there are regions with high and low visitation frequency as indicated by the density of the points of the attractor (Fig. 19.12a). The density of the attracting space reflects the amount of information needed to describe the state of the system. Referring to Fig. 19.12b the following gives an ecological interpretation of the attractor densities for the different phases of the virgin forest development cycle.

(i) Regeneration: During regeneration, the open canopy space becomes occupied by new plants and the C source strength of the ecosystem declines. The competition for light and nutrients is low and little information is required to predict the development of the ecosystem.

(ii) Adolescence: With adolescence, the ecosystem achieves canopy closure and enters a stationary phase with small fluctuations between C sink and C source. The competition for light becomes important and individual tree competition is evident. More information is required to understand which individuals will survive and which will die.

(iii) Optimum: When the ecosystem enters the optimum phase it becomes a net C sink. The individuals that survived adolescence grow at different rates and small differences in nutrient or light availability are important for the competitive situation of a tree within the stand. The amount of information needed to predict the performance of individual trees is at its maximum. At the peak of the optimum phase, C sink strength is at its maximum and the most successful individuals dominate the ecosystem. The amount of information needed to predict ecosystem performance starts to decrease.

(iv) Old Growth: The maintenance costs of the accumulated biomass increase during the old growth phase. In years with unfavorable climate conditions single individuals die due a negative individual carbon balance. The ecosystem enters another stationary phase with small fluctuations between carbon sink and carbon source.

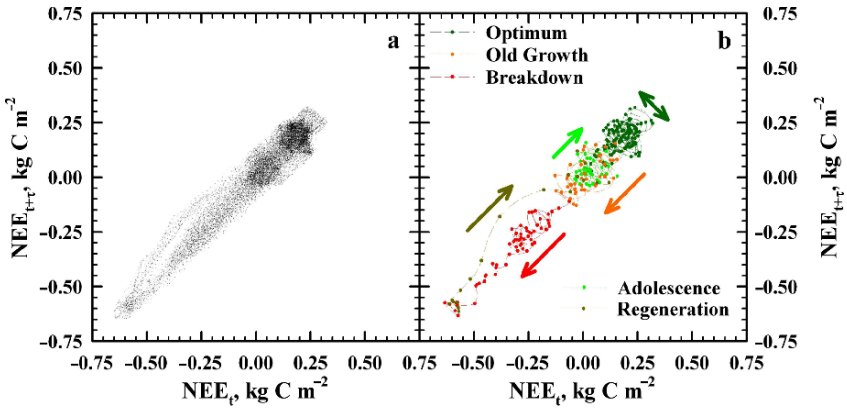

Fig. 19.12. Attractor of modeled NEE for the successional cycle evident within the virgin forest reserve Rothwald. **a**: NEE-Attractor for the virgin forest successional cycle reconstructed from model results using site and climate conditions of 18 research plots. **b**: Attractor reconstructed for one single plot and one successional cycle. Arrows indicate the trends of model behavior during different phases of the successional cycle. (S.A. Pietsch, unpublished) See also Color Plates, Fig. 6

The amount of information needed to describe the system increases compared to the optimum phase.

(v) Breakdown: During this phase individuals collapse under the maintenance costs of their biomass and the ecosystem becomes a net C source. This process accelerates with time and less information is needed to predict ecosystem behavior. This is evident from the decreasing attractor density towards the peak of C source strength.

A visual analysis of the attractor reconstructed from an ecosystem level process (NEE) provides information on the individuals constituting the ecosystem. This is an important result showing that a process resulting from the sum of the behavior of individuals also contains information on the individuals. This information is of practical value for the determination of sample size in field studies. If an ecosystem is in phase with high attractor density, then a higher number of samples will be needed to gather the amount of information necessary to understand dynamics of the ecosystem. If the ecosystem is in a phase with low attractor density, then a smaller sample size will be necessary to understand the dynamics of the ecosystem. Ergodic theory provides a link between the process-based description of an ecosystem and the statistical description of the individuals residing within this ecosystem.

VI. Concluding Remarks

Large-scale ecosystem models describe the transformation of energy and matter within an ecosystem. Among the processes determining the fluxes of energy and matter, photosynthesis has the central role and is the key of the interactions between the carbon, water, nitrogen and energy cycle. Photosynthesis interacts with the water cycle by the trade-off between carbon uptake and water loss across leaf stomata. Photosynthesis is linked to the nitrogen cycle by the high proportion of leaf nitrogen allocated to the carbon fixing enzymes Rubisco and PEP-Carboxylase. The energy cycle is influenced by photosynthesis via solar shortwave radiation absorption, which fuels photosynthetic electron transport rate.

Complex large scale ecosystem models link photosynthesis with processes of plant growth and decay. In this context the models serve as diagnostic tools to assess and understand observed ecosystem carbon, water and nutrient dynamics. Comparisons of model predictions on states and fluxes with field observations are essential for testing the formal implementation of ecosystem processes. This is paramount for ensuring a realistic representation of reality over time periods, starting from days to seasons (Figs. 19.8–19.10, Section V.B.) and continuing to complete ecosystem life cycles (Fig. 19.6, Section V.A).

Model validations require independent observations covering the full variation range of ecosystem development stages. Data should include different site and climate conditions across the ecosystems distribution range. Validation is the key step in assessing the error component of model applications (i.e. the accuracy and precision of model predictions; see Section IV.C). Validation allows the comparison of prediction uncertainty with observed variation. When prediction uncertainty exceeds observed variation, an expert guess may be more accurate than a model application.

Validations of complex large-scale ecosystem models form the backbone for any scenario analyses. After rigorous model validation, one final important question remains: How reliable are model predictions beyond the range of conditions prevalent during the validation process?

A possible solution to this problem may be an analysis of model dynamics using methods from ergodic theory (Section IV.D) If the model dynamics remain stable under a given scenario (e.g. climate change), then model predictions may be considered as feasible.

Currently, we understand the major relations among ecosystem processes ranging from photosynthesis to decomposition. The implementation of the processes in a formal model allows us to mimic nature and to determine the accuracy and precision of model predictions. For the future, we will have to investigate the relationship between model dynamics and real world ecosystem dynamics (Sections IV.D and V.C). Such understanding may enable us to evaluate the quality of model predictions on future ecosystem behavior as it may develop with changing climate.

Acknowledgments

This research was funded by the Austrian Science Foundation (FWF) project number P20660-B16 (Ergodic theories within Ecosystem Modeling), the Austrian Federal Ministry of Science and Education (BMWF), the Austrian Federal Ministry of Agriculture, Forestry, Environment and Water Management (BMLFUW) and the Austrian Federal Ministry of Transport, Innovation and Technology (BMVIT). We thank Agu Laisk for helpful comments on the chapter.

References

Aber JD (1992) Nitrogen cycling and nitrogen saturation in temperate forest ecosystems. Trends Ecol Evol 7: 220–22

Andren O and Paustian K (1987) Barley straw decomposition in the field: a comparison of models. Ecol 68: 1190–1200

Assmann E (1970) The Principles of Forest Yield Study. Pergamon Press, Oxford

Bachelet D, Lenihan J, Daly C, Neilson R, Ojima D and Parton W (2001) MC1: a dynamic vegetation model for estimating the distribution of vegetation and associated ecosystem fluxes of carbon, nutrients, and water. USDA Forest Service, Pacific Northwest Station, Gen Tech Rep PNW-GTR-508

Boltzmann, L (1877) Über die Beziehung zwischen dem zweiten Hauptsatze der mechanischen Wärmetheorie und der Wahrscheinlichkeitsrechnung respektive den Sätzen über das Wärmegleichgewicht. Wiener Berichte 76: 373–435

Broer H, Simó C and Vitolo R (2002) Bifurcations and strange attractors in the Lorenz-84 climate model with seasonal forcing. Nonlinearity 15: 1205–1267

Brooks RH and Corey AT (1964) Hydraulic properties of porous media. Hydrology Papers 3, Colorado State University, Fort Collins, CO

Carbone G (2007) Exercises in Weather and Climate, 6th ed, Prentice-Hall, Upper Saddle River, NJ

Chang M (2003) Forest Hydrology: An Introduction to Water and Forests. CRC Press LLC, Boca Raton, FL

Clapp RB and Hornberger GM (1978) Empirical equations for some soil hydraulic properties. Water Resource Res 14: 601–604

Collins WJ, Derwent RG, Johnson CE and Stevenson DS (2002) A comparison of two schemes for the convective transport of chemical species in a Lagrangian global chemistry model. Quart J Royal Meteo Soc 128: 991–1009

Cosby BJ, Hornberger GM, Clapp RB and Ginn TR (1984) A statistical exploration of the relationships of soil moisture characteristics to the physical properties of soils. Water Resource Res 20: 682–690

de Pury DGG and Farquhar GD (1997) Simple scaling of photosynthesis from leaves to canopies without the errors of big-leaf models. Plant Cell Environ 20: 537–557

Eckmann J-P and Ruelle D (1985) Ergodic theory of chaos and strange attractors. Rev Modern Phys 57: 617–656

Etheridge DM, Steele LP, Langenfelds RL, Francey RJ, Barnola J-M and Morgan VI (1996) Natural and anthropogenic changes in atmospheric CO_2 over the last 1000 years from air in Antarctic ice and firn. J Geophys Res 101: 4115–4128

Evans JR (1989) Photosynthesis and nitrogen relationships in leaves of C_3 plants. Oecologia 78: 9–19

Farquhar G, Von Caemmerer S and Berry J (1980) A biochemical model of photosynthetic CO_2 fixation in leaves of C_3 species. Planta 149: 78–90

Finzi A and Schlesinger WH (2002) Species control variation in litter decomposition in a pine forest exposed to elevated CO_2. Global Change Biol 8: 1217–1229

Harcomb PA (1987) Tree life tables: Simple birth, growth and death data encapsulate life histories and ecological roles. Bioscience 37: 557–568

Hasenauer H, MerganiÃĺová K, Petritsch R, Pietsch SA and Thornton PE (2003) Validating daily climate interpolations over complex terrain in Austria. Agric Forest Meteorol 119: 87–107

Heinselman ML (1973) Fire in the virgin forests of the boundary waters canoe area, Minnesota. Quaternary Res 3: 329–382

Holland EA, Dentener FJ, Braswell BH and Sulzman JM (1999) Contemporary and pre-industrial global nitrogen budgets. Biogeochem 46: 7–43

Keeling CD, Bacastow RB, Carter AF, Piper SC, Whorf TP, Heimann M, Mook WG and Roeloffzen H (1989). A three-dimensional model of atmospheric CO_2 transport based on observed winds: 1. Analysis of observational data. In: Peterson DH (ed) Aspects of Climate Variability in the Pacific and the Western Americas. Geophys Monogr 55: 165–235

Krinner G, Viovy N, de Noblet-Ducoudré N, Ogée J, Polcher J, Friedlingstein P, Ciais P, Sitch S and Prentice C (2005) A dynamic global vegetation model for studies of the coupled atmosphere-biosphere system. Global Biogeochem Cycles 19: GB1015

Kuehn GD and McFadden BA (1969) Ribulose 1,5-diphosphate carboxylase from *Hydrogenomonas eutropha* and *Hydrogenomonas facilis*. I. Purification, metallic ion requirements, inhibition, and kinetic constants. Biochemistry 8: 2394–2402

Laisk A and Edwards GE (2000) A mathematical model of C_4 photosynthesis: The mechanism of concentrating CO_2 in NADP-malic enzyme type species. Photosynth Res 66: 199–224

Lloyd J and Taylor JA (1994) On the temperature dependence of soil respiration. Funct Ecol 8: 315–323

Lorimer CG, Dahir SE and Nordheim EV (2001) Tree mortality rates and longevity in mature and old growth hemlock hardwood forests. J Ecol 89: 960–971

Mayer H and Ott E (1991) Gebirgswaldbau-Schutzwaldpflege. Fischer Verlag, Stuttgart

Melillo JM, McGuire AD, Kicklighter DW, Moore III B, Vorosmarty CJ and Schloss AL (1993) Global climate change and terrestrial net primary production. Nature 363: 234–240

Melillo JM, Kicklighter DW, McGuire AD, Peterjohn WT and Newkirk KM (1995) Global change and its effects on soil organic carbon stocks. In: Zepp RG and Sonntag Ch (eds) Role of Nonliving Organic Matter in the Earth's Carbon Cycle, pp 175–189. Wiley, Chichester

Merganičova K, Pietsch SA and Hasenauer H (2005) Modeling the impacts of different harvesting regimes on the growth of Norway spruce stands. Forest Ecol Manag 207: 37–57

Monserud RA and Sterba H (2001) Modeling individual tree mortality for Austrian tree species. Forest Ecol Manag 113: 109–123

Ott E, Frehner M, Frey H-U and Löscher P (1997) Gebirgswälder-Ein Praxisorientierter Leitfaden für Standortgerechte Waldbehandlung. Paul Haupt Verlag, Bern

Penning de Vries FWT (1974) Substrate utilization and respiration in relation to growth and maintenance in higher plants. Netherlands J Agric Sci 22: 40–44

Peterken GF (1996) Natural Woodland: Ecology and Conservation in Northern Temperate Regions. Cambridge University Press, Cambridge

Petit JR, Basile I, Leruyuet A, Raynaud D, Lorius C, Jouzel J, Stievenard M, Lipenkov VY, Barkov NI, Kudryashov BB, Davis M, Saltzman E and Kotlyakov V (1997) Four climate cycles in Vostok ice core. Nature 387: 359–360

Petit JR, Jouzel J, Raynaud D, Barkov NI, Barnola J-M, Basile I, Bender M, Chappellaz J, Davis M, Delayque G, Delmotte M, Kotlyakov VM, Legrand M, Lipenkov VY, Lorius C, Pépin L, Ritz C, Saltzman E and Stievenard M (1999) Climate and atmospheric history of the past 420,000 years from the Vostok ice core, Antarctica. Nature 399: 429–436

Petritsch R and Hasenauer H (2007) Interpolating input parameters for large scale ecosystem models. Aust J Forest Sci 124: 135–151

Pietsch SA and Hasenauer H (2002) Using mechanistic modeling within forest ecosystem restoration. Forest Ecol Manag 159: 111–131

Pietsch SA and Hasenauer H (2003) Stoffkreislaufmodellierung im Grasland: Machbarkeitsstudie für die Adaptierung eines biogeochemisch mechanistischen Modells. Inst. of Forest Growth Research, Vienna

Pietsch SA and Hasenauer H (2005a) Using ergodic theory to assess the performance of ecosystem models. Tree Physiol 25: 825–837

Pietsch SA and Hasenauer H (2005b) Modeling Cembran pine forerst ecosystems in Austria. Aust J Forest Sci 122: 37–54

Pietsch SA and Hasenauer H (2006) Evaluating the self-initialization procedure of large scale ecosystem models. Global Change Biol 12: 1658–1669

Pietsch SA, Hasenauer H, Kučera J and Čermák J (2003) Modeling effects of hydrological changes on the carbon and nitrogen balance of oak in floodplains. Tree Physiol 23: 735–746

Pietsch SA, Hasenauer H and Thornton PE (2005) BGC-Model parameter sets for central European forest stands. Forest Ecol Manag 211: 264–295

Poincaré H (1892) Les Méthodes Nouvelles de la Mécanique Céleste. Vol. 1: Solutions Périodiques, Non-Existence des Méthodes Uniformes, Solutions Asymptotiques. Gauthier-Villars, Paris

Popper KR (1935) Logik der Forschung. Zur Erkenntnistheorie der Modernen Wissenschaft. Julius Springer, Wien

Racsko P, Szeidl L and Semenov MA (1991) A serial approach to local stochastic weather models. Ecol Modell 57: 27–41

Remmert H (1991) The Mosaic Cycle Concept of Ecosystems. Ecological Studies 85. Springer, Berlin

Reynolds MR Jr (1984) Estimating the error in model predictions. Forest Sci. 30: 454–469

Richardson CW and Wright DA (1984) WGEN: A Model for Generating Daily Weather Variables. US Department of Agriculture, Agricultural Research Service, ARS-8

Ruelle D (1978) Sensitive dependence on initial condition and turbulent behaviour of dynamical systems. Ann NY Acad Sci 316: 408–416

Ruelle D (1995) Turbulance, strange attractors and chaos. World Scientific Series on Non-linear Science, Series A Vol 16, World Scientific Press, Singapore

Ryan MG (1991) Effects of climate change on plant respiration. Ecol Applicat 1: 157–167

Saxton KE, Rawls WJ, Romberger JS and Papendick RI (1986) Estimating generalized soil-water characteristics from texture. Soil Sci Soc Am J 50: 1031–1036

Scheffer M, Carpenter S, Foley JA, Folke C and Walker B (2001) Catastrophic shifts in ecosystems. Nature 413: 591–596

Schlesinger WH (1997) Biogeochemistry: An Analysis of Global Change, 2nd ed, Academic, San Diego, CA

Schneider J (1998) Kartierung der nassen Deposition in Österreich. Umweltbundesamt Wien

Semenov MA, Brooks RJ, Barrow EM and Richardson CW (1998) Comparison of WGEN and LARS-WG stochastic weather generators for diverse climates. Clim Res 10: 95–107

Sitch S, Smith B, Prentice IC, Arneth A, Bondeau A, Cramer W, Kaplan JO, Levis S, Lucht W, Sykes MT, Thonicke K and Venevsky S (2003) Evaluation of ecosystem dynamics, plant geography and terrestrial carbon cycling in the LPJ dynamic global vegetation model. Global Change Biol 9: 161–185

Spiecker H, Hanse J, Klimo E, Skovsgaard, JP, Sterba H, Von Teuffel K (2004) Norway spruce conversion – options and consequences. European Forest Institute Research Report. S. Brill Academic, Leiden/Bosten/Köln

Takens F (1981) Detecting strange attractors in turbulence. In: Rand D and Young L-S (eds) Dynamical Systems and Turbulence, pp 366–381. Springer, Berlin

Thornton PE (1998) Description of a Numerical Simulation Model for Predicting the Dynamics of Energy, Water, Carbon and Nitrogen in a Terrestrial Ecosystem. Ph.D.-thesis. University of Montana, Missoula, MT

Thornton PE, Hasenauer H and White MA (2000) Simultaneous estimation of daily solar radiation and humidity from observed temperature and precipitation: An application over complex terrain in Austria. Agric Forest Meteor 104: 255–271

Tiedtke M (1989) A comprehensive mass flux scheme for cumulus parameterization in large-scale models. Monthly Weather Rev. 117: 1779–1800

Ulrich E and Williot B (1993) Les Dépôts Atmosphériques en France de 1850 à 1990, Dépôts en Milieu Rural et en Fôret, Dépôts dans les Zones Industrialisées et Urbaines. Imprimiere de l'Office National des Forêts, Paris

Waring RH and Running SW (1998) Forest Ecosystems: Analysis at Multiple Scales, 2nd ed, Academic, San Diego, CA

White MA, Thornton PE, Running SW and Nemani RR (2000) Parameterization and sensitivity analysis of the BIOME-BGC terrestrial ecosystem model: Net primary production controls. Earth Interactions Paper 4–003. http://EarthInteractions.org

Woodrow IE and Berry JA (1980) Enzymatic regulation of photosynthetic CO_2 fixation in C_3 plants. Annu Rev Plant Physiol Plant Mol Biol 39: 533–594

Wullschleger SD (1993) Biochemical limitations to carbon assimilation in C_3 plants – A retrospective analysis of the A/C_i curves from 109 species. J Exp Bot 44: 907–920